Chapter 2
Angiogenesis and Vascular Remodeling in Inflammation and Cancer: Biology and Architecture of the Vasculature

Donald M. McDonald

Keywords: angiogenesis, angiogenesis inhibitors, basement membrane, endothelial cells, pericytes, tumors, plasma leakage, vascular permeability, vascular remodeling, VEGF

Abstract: Blood vessels proliferate by sprouting from existing vessels (angiogenesis) and undergo changes in phenotype (vascular remodeling) in inflammatory diseases, tumors, and many other chronic conditions. Changes in newly formed and remodeled blood vessels are disease-specific, as they reflect vascular adaptations to environmental cues unique to each condition. In inflamed tissues, vascular remodeling expands the vasculature and increases blood flow, plasma leakage, and inflammatory cell influx, which contribute to the pathophysiology and clinical manifestations of the disease. Remodeling of endothelial cells into a venular phenotype, typical of sustained inflammation, is accompanied by expression of molecules that promote endothelial gap formation and leukocyte rolling, attachment, and migration. Blood vessels in tumors differ from those in inflammation. Endothelial cells in tumors undergo disorganized sprouting, proliferation and regression, and become dependent on vascular endothelial growth factor (VEGF) or other factors for survival. The growing vasculature enables tumor enlargement, but structural defects impair endothelial barrier function and increase interstitial pressure and luminal resistance, diminish blood flow, and alter immune cell traffic. Oxygen delivery may be inadequate for tumor cell viability despite the rich vascularity. Inhibition of VEGF signaling in tumors stops sprouting angiogenesis and triggers regression of some tumor vessels while normalizing others. Some capillaries in normal thyroid, pancreatic islets, and intestine may also regress after VEGF blockade, but most remodeled vessels at sites of inflammation do not. Pericytes and empty sleeves of vascular basement membrane persist after endothelial cells regress and provide a scaffold for blood vessel regrowth, which can occur within days after the inhibition ends. The clinical efficacy of VEGF signaling inhibitors in cancer and age-related macular degeneration provides proof of concept and stimulates the search for even more effective agents. Further advances in vascular biology will lead to more powerful strategies for controlling blood vessel growth and regression in health and disease.

Comprehensive Cancer Center, Cardiovascular Research Institute, and Department of Anatomy, University of California, San Francisco, CA, USA

Address for Correspondence:
Department of Anatomy, University of California, Room S-1363, 513 Parnassus Avenue, San Francisco, CA, USA
E-mail: donald.mcdonald@ucsf.edu

Introduction

During normal body growth and in many disease processes, blood vessels proliferate by angiogenesis, where new vessels sprout from existing ones. The expanding vasculature provides nutrients to enlarging tissues and routes for cells to leave or enter the circulation. Blood vessels can also undergo remodeling, whereby they acquire a new phenotype manifested by changes in structural and functional properties.

Normal blood vessels are lined by a monolayer of thin, smooth, tightly joined endothelial cells that form the barrier that controls the transendothelial flux of water, solutes, and cells. The endothelial cells rarely sprout or divide. Vascular stability results in part from the intimate association of mural cells (pericytes or smooth muscle cells) with the abluminal surface of endothelial cells. Endothelial cells and mural cells, which together generate a tight envelopment of basement membrane, form a stable, functional unit.

Blood vessels of the normal microcirculation are organized into a hierarchy of arterioles, capillaries, and venules, each having distinctive structural and functional characteristics [1]. This hierarchical organization is superimposed on organ-specific specializations of the blood vessels. As a result, blood vessels of different organs have some features in common and some that are unique to each organ.

Newly formed or remodeled blood vessels in most pathological conditions differ from normal vessels at multiple levels.

Abnormalities range from altered activity of receptors, adhesion molecules, or signaling pathways, to loss of hierarchical organization, and to widespread changes in three-dimensional architecture [2]. In inflammation, the types of blood vessels that are sources of plasma leakage and leukocyte efflux expand by remodeling and angiogenesis [3–5]. Vascular specialization progresses as inflammation evolves and becomes an integral part of the inflammatory response. Of the four cardinal signs of inflammation—rubor, tumor, calor, and dolor—the first three reflect changes in the vasculature.

Abnormalities in tumor blood vessels differ from the changes in inflammation. The endothelial cells in tumors undergo disorganized sprouting, proliferation and regression, and may be dependent on growth factors for survival [1, 2]. Despite extensive angiogenesis in tumors, structural defects lead to leakiness, high luminal resistance, poor blood flow, altered trafficking of immune cells, and elevated interstitial pressure. Blood flow may be inadequate to support tumor cell viability despite dense vascularity.

This chapter reviews the evolution of approaches we have developed or adapted to obtain a better understanding of changes in three-dimensional vascular architecture, vascular phenotype and hierarchy, and the cell biology of endothelial cells and pericytes in vivo. The strategy was first to understand the properties of a relatively simple vascular network under baseline conditions and then to determine how the vasculature changed under pathological conditions. Models in mice or rats were used to compare angiogenesis and vascular remodeling in chronic inflammation and cancer. As expected, the learning process has been evolutionary, with each stage building on previous ones. Progress has enabled, step by step, the development of more informative methods, analysis of more complex systems, and investigation of more complex issues in the in vivo setting.

Approaches for Detecting Changes in Vascular Architecture

With the goal of developing more effective ways of detecting alterations in the three-dimensional architecture and cellular changes in blood vessels under conditions that lead to angiogenesis and vascular remodeling, we sought better approaches for visualizing the microvasculature [6, 7]. As a starting point, we adapted the historical method of using silver nitrate to stain the borders of endothelial cells of blood vessels in situ (Fig. 2.1A, B) and exploited the simple segmented vascular architecture of the murine trachea as a test system (Fig. 2.1B inset) [6]. Once stained, the preparations could be examined as three-dimensional whole mounts, where all segments of the microvasculature—arterioles, capillaries, and venules—could be identified. This system had the additional attribute of making it possible to pinpoint sites of leakage at the cellular level. Leaky sites were found to coincide with gaps between endothelial cells of postcapillary venules (Fig. 2.1C, D) [6].

As a technically easier and more flexible approach, we explored the binding properties of plant lectins for labeling the vascular endothelium in situ, again using the vasculature of the rat trachea as a test system [7]. *Lycopersicon esculentum* (LEA) lectin, which has a primary specificity for *N*-acetyl-D-glucosamine oligomers, was found to bind strongly and uniformly to the luminal surface of endothelial cells when administered by intravenous (iv) injection or vascular perfusion. Of the 20 lectins tested in this system, *Solanum tuberosum* (STL) and *Datura stramonium* (DSL), which also bind *N*-acetyl-D-glucosamine oligomers, had properties similar to LEA. Later experiments revealed that *Griffonia (Bandeiraea) simplicifolia* I (GSL-I) isolectin B4 effectively labels the vasculature of mice after iv injection with less toxicity than LEA. Biotinylated lectins were visualized by avidin-peroxidase histochemistry (Fig. 2.2A, B) and fluorescent lectins by fluorescence microscopy or confocal microscopy. Because of uniform binding, LEA lectin revealed the overall architecture of the vasculature (Fig. 2A, B) and amazingly detailed features of the luminal surface [3, 7]. *Triticum vulgaris* lectin (Wheat germ agglutinin, WGA) did not bind uniformly but had the distinctive property of binding strongly to endothelial cells of capillaries and arterioles but not postcapillary venules (Fig. 2A inset) [7]. By comparison, *Ricinus communis* agglutinin I lectin bound only weakly to the vasculature but clearly marked leaky sites by binding intensely to the extracellular matrix in regions of extravasation [4, 7].

Vascular Remodeling and Angiogenesis in Inflammation

Staining the luminal surface of the endothelium with biotinylated or fluorescent LEA lectin proved useful in characterizing vascular changes in chronic inflammation in the respiratory tract of rats (Fig. 2.2A, B) and mice (Fig. 2.2C, D). This approach provides an overview of the vascular architecture and the number and location of adherent intravascular leukocytes [5, 8, 9]. In this way, angiogenesis and vascular remodeling were found to be prominent features of the inflammatory response of the airway mucosa after infection by the respiratory pathogen *Mycoplasma pulmonis* [5, 8, 9]. This infection is known to lead to chronic airway inflammation in rats and mice [10–12]. Unlike normal vasculature, blood vessels that undergo remodeling after *M. pulmonis* infection are leaky, and the leakiness is greatly exaggerated by the inflammatory mediator substance P (Fig. 2.2Binset), because of up-regulation of neurokinin-1 receptors on endothelial cells [13, 14]. Remodeled capillaries acquire a venular phenotype, with increased expression of molecules typical of inflamed venules, including P-selectin, E-selectin, EphB4, and ICAM-1. These changes lead to selective expansion of a specialized population of blood vessels (venules) that support plasma leakage and leukocyte influx (Fig. 2.2D). The model of experimental *M. pulmonis* infection makes it possible to examine the mechanism, consequences, and reversibility of angiogenesis and vascular remodeling in sustained inflammation.

The overall architecture of the tracheal vasculature changes dramatically after *M. pulmonis* infection. The magnitude of

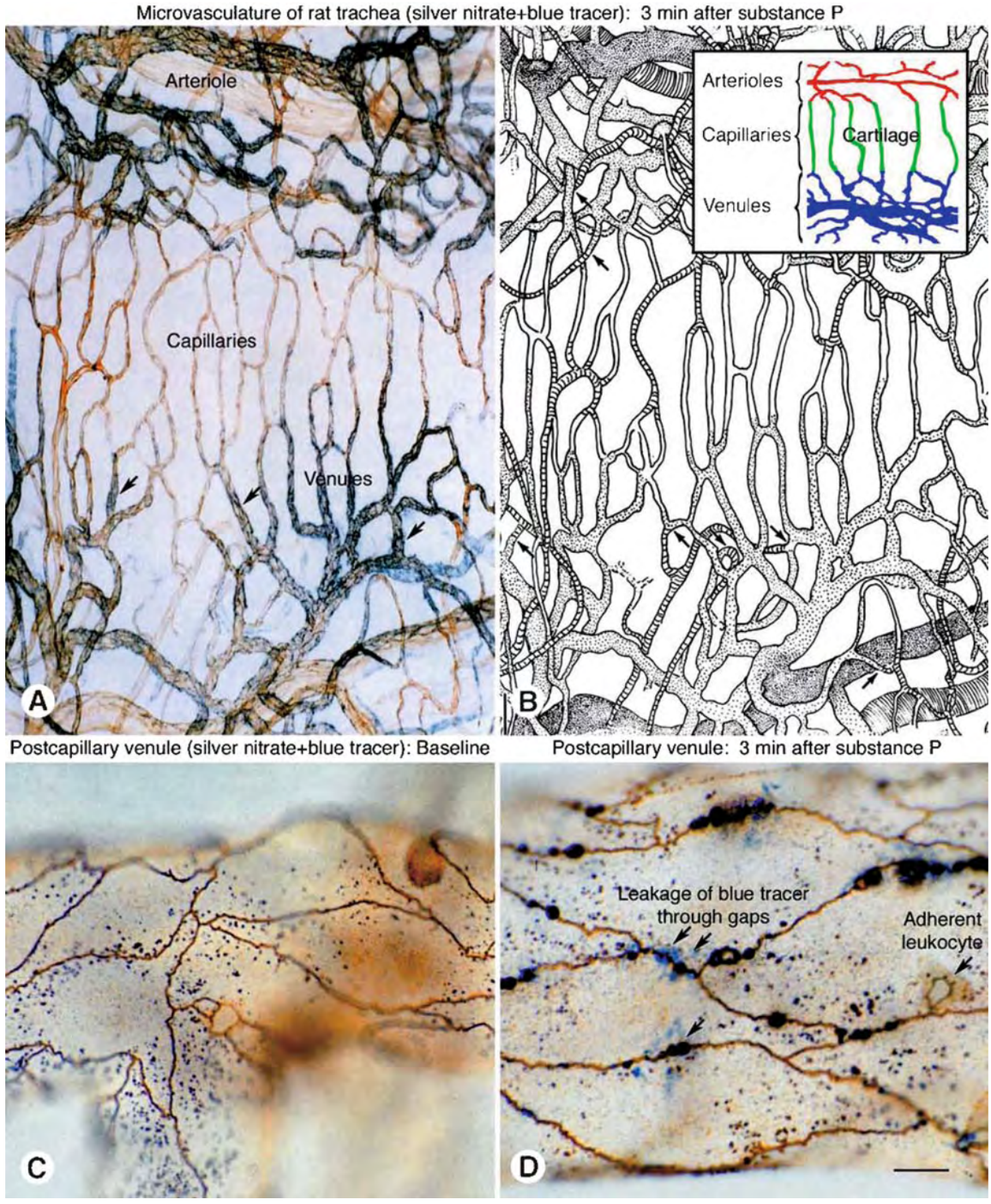

FIG. 2.1A–D. Light micrograph (**A**) and corresponding drawing (**B**) of vasculature of rat tracheal mucosa after injection of particulate blue tracer, Monastral blue, and leak-inducing substance P (5 µg/kg iv) followed 3 min later by removal of intravascular tracer by vascular perfusion of fixative and staining of endothelial cells in situ with silver nitrate (from [6]). Postcapillary venules in (**A**) are labeled by extravasated Monastral blue, reflecting sites of substance P-induced leakage. Capillaries are not labeled. The drawing identifies six types of blood vessels distinguished by endothelial cell morphology: segmental arterioles *(long contour lines*), terminal arterioles (*short contour lines*), arteriovenous anastomoses (*arrows*), capillaries (*unmarked*), postcapillary venules (*light stipple*), and collecting venules (*heavy stipple*). **B** (*inset*) Schematic of vascular architecture, with most capillaries over cartilage rings and other vessels between the rings. **C, D** Light micrographs showing borders of endothelial cells of postcapillary venule of rat trachea after silver nitrate staining under baseline conditions (**C**) and after substance P (**D**) (5 µg/kg iv, 3 min) (from [3]). Dot-like silver deposits (*arrows*) at endothelial cell borders mark intercellular gaps (**D**). Patches of extravasated Monastral blue (*arrows*) mark sites of leakage (**D**). Adherent leukocyte (**D** *arrowhead*). *Scale bar*: 100 µm in (**A,B**); 10 µm in (**C, D**).

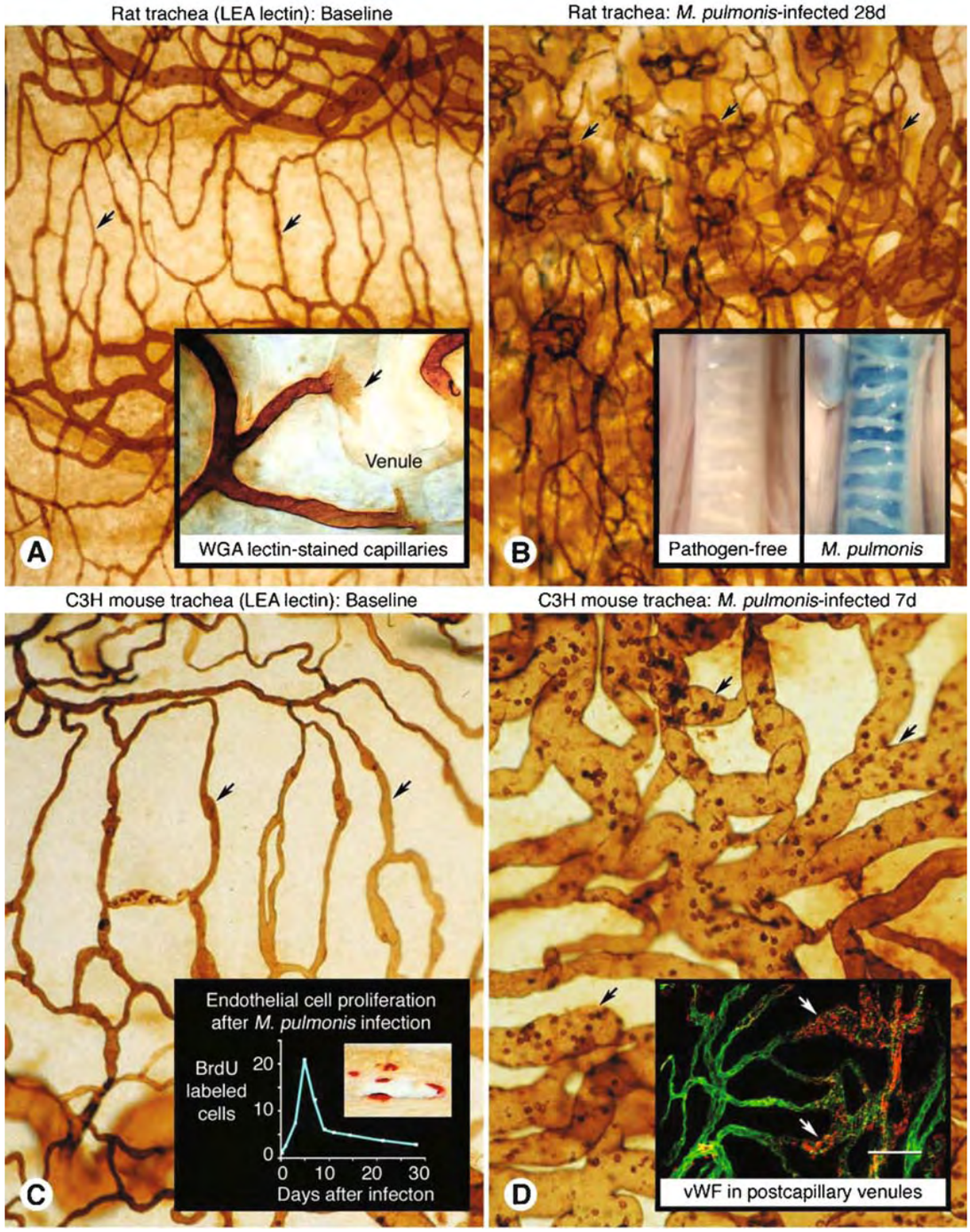

FIG. 2.2A–D. Comparison of vasculature in tracheal mucosa under baseline conditions (pathogen-free) and after *M. pulmonis* infection in rats (**A,B**) and mice (**C,D**). Blood vessels stained by perfusion of LEA lectin. Simple pattern of tracheal vasculature in pathogen-free rat, with relatively straight capillaries (**A** *arrows*), compared to tortuous networks of new vessels (**B** *arrows*) in trachea of rat infected with *M. pulmonis* for 4 weeks. **A** (*inset*) Strong binding of WGA lectin to endothelial cells of capillary (*arrow*) next to weak binding to endothelial cells of venule in rat trachea (from [7]). **B** (*inset*) Exaggerated substance P-induced plasma leakage in rat trachea after *M. pulmonis* infection. Pale trachea reflects little Monastral blue leakage in pathogen-free trachea (*left*) compared to extensive leakage after *M. pulmonis* infection for 4 weeks (*right*). Both tracheas prepared 2 min after iv injection of capsaicin (75 µg/kg) to evoke release of endogenous substance P (from [12]). Simple network of tracheal capillaries (**C** *arrows*) in pathogen-free mouse compared to capillaries enlarged and remodeled into venules with abundant adherent leukocytes (**D** *arrows*) in C3H mouse infected with *M. pulmonis* for 8 weeks (from [5]). **C** (*inset*) Time course of endothelial cell proliferation assessed by BrdU labeling of tracheal mucosa of *M. pulmonis*-infected C3H/HeN mice (from [18]). Micrograph shows BrdU-labeled cells localized by immunohistochemistry (*red*) in C3H mouse infected for 1 week (from [9]). **D** (*inset*) Confocal micrograph showing von Willebrand factor (vWf)-immunoreactivity (*red*) in endothelial cells of tracheal blood vessels in C3H mouse infected with *M. pulmonis* for 4 weeks (from [8]). Vasculature stained by perfusion of green fluorescent LEA lectin. vWf immunoreactivity is strongest in venules (*arrows*). *Scale bar*: 150 µm in (**A,B**); 75 µm in (**C,D**); 50 µm in (**A** *inset*); 5 mm in (**B** *inset*); 50 µm in (**C** *inset*); 100 µm in (**D** *inset*).

the changes corresponds to the severity of the infection. Some strains of mice develop more severe disease than others [15, 16]. Relative amounts of angiogenesis and vascular remodeling also vary among strains [8]. Vascular remodeling, in which mucosal blood vessels can double in size without much increase in number, predominates in C3H mice (Fig. 2.2C, D), but angiogenesis and vascular remodeling are both conspicuous in C57BL/6 mice and in rats after *M. pulmonis* infection [8, 14, 17].

Vascular remodeling after *M. pulmonis* infection is manifested by enlargement of capillaries and venules, and less so arterioles. The enlargement results from endothelial cell proliferation, not vasodilatation. Endothelial cell size is preserved. The rate of endothelial cell proliferation, determined by BrdU uptake, begins to increase a few days after infection, peaks at 5 days with a value 18 times baseline (pathogen-free), declines somewhat through day 9, and remains at 3 times the pathogen-free value for at least 28 days (Fig. 2.2C inset) [18]. Through selective expression of adhesion molecules, remodeled vessels become sites of leukocyte adherence (Fig. 2. 2D). This remodeling of the microvasculature occurs at an early stage of inflammation, considerably before widespread tissue remodeling.

Staining of blood vessels with a lectin is made more informative by concurrent immunohistochemical staining of endothelial cells, pericytes, and adjacent cells in three-dimensional tracheal whole mounts [4, 19–23]. This approach has the attribute of showing the amount and location of angiogenesis and vascular remodeling in the context of inflammatory cells, lymphatic vessels, and specific enzymes, growth factors, receptors, adhesion molecules, or matrix elements [21–23]. For example, preferential expression of von Willebrand factor (vWf) in venules is apparent when vWf immunoreactivity is combined with lectin staining (Fig. 2.2D inset).

Staining for platelet endothelial cell adhesion molecule-1 (PECAM-1, CD31) and lymphatic vessel endothelial hyaluronan receptor (LYVE-1) reveals the three-dimensional architecture of blood vessels and lymphatic vessels and the prominent changes both undergo after *M. pulmonis* infection (Fig. 2.3A–C) [23]. In comparison to blood vessel remodeling, which is greatest during the first week after infection, lymphatics begin to grow during the second week (Fig. 2.3B) [23], and by 28 days are more abundant than blood vessels in the inflamed airway mucosa (Fig. 2.3C) [23]. Growth of lymphatic vessels can be blocked by inhibition of vascular endothelial growth factor (VEGF) receptor-3 signaling. However, remodeling (enlargement) of blood vessels is not prevented by inhibition of VEGFR1, VEGFR-2, and/or VEGFR-3 [23].

Reversibility of Angiogenesis and Vascular Remodeling in Inflammation

Vascular remodeling after *M. pulmonis* infection is not blocked by inhibition of VEGF signaling [23]. However, it can be reversed by reducing the inflammatory and immunologic response with dexamethasone or by reducing the number of organisms with oxytetracycline [17, 19]. After infection with *M. pulmonis* for 6 weeks, the simple vasculature of the rat tracheal mucosa (Fig. 2.3D) is unrecognizably changed by chaotic angiogenesis (Fig. 2.3E). But daily treatment with dexamethasone or oxytetracycline for 4 weeks leads to almost complete resolution of the angiogenesis and vascular remodeling (Fig. 2.3F) [17].

Similarly, tracheal capillaries of C3H mice infected with *M. pulmonis* change from their conventional narrow caliber and absence of adherent leukocytes (Fig. 2.3G) to conspicuously enlarged vessels that have a venular phenotype, high P-selectin expression, and abundant adherent leukocytes (Fig. 2.3H) [19]. Treatment with dexamethasone for a week reverses the vascular enlargement, venular transformation, and leukocyte adherence (Fig. 2.3I) [19].

The driving force for vascular remodeling after *M. pulmonis* infection has not been identified, but existing evidence indicates that VEGF receptor activation is not essential [23]. Perhaps relevant to the alternatives, airway capillaries become conspicuously enlarged in mice treated with angiopoietin-1, its mimic, COMP-Ang1, or angiopoietin-2 [24–26]. These ligands signal through Tie2 receptors. The transformed vessels have a venular phenotype with similarities to the remodeled vasculature after *M. pulmonis* infection [8, 9]. This phenotype has also been reported in venous malformations resulting from point mutations accompanied by constitutive Tie2 activation [27, 28]. How the role, if any, of Tie2 activation after *M. pulmonis* infection fits with the actions of tumor necrosis factor, interleukins, and other cytokines [29, 30] must still be determined.

Abnormalities of Blood Vessels in Tumors

Identification of tumor vessels

Blood vessels in tumors have bizarre defects unlike those in inflammation. Endothelial cells, pericytes, and the vascular basement membrane are all abnormal [1, 2, 31, 32]. Tumor vessels are so unusual that even their identification as blood vessels can be challenging. Do tumor vessels include strands of endothelial cells regardless of whether they have a lumen and are routes for blood flow? Are all routes of blood flow in tumors lined by endothelial cells? Do collections of erythrocytes without accompanying endothelial cells mark sites of blood flow or sites of hemorrhage? These questions have stimulated innovative hypotheses, novel experiments, and much debate [33–38].

From the perspective of mammalian vascular biology, blood vessels in tumors are the channels for blood circulation. Channels continuously connected to the circulation do not include extravascular pathways for movement of extravasated fluid or collections of extravasated erythrocytes. With this definition, how can capillary-sized blood vessels be identified unambiguously in the abnormal setting of tumors? The most straightforward method is intravital imaging of flowing blood through vessels in tumors [39]. Intravital imaging is nicely complemented by confocal microscopic imaging of tissues preserved by perfusion fixation and stained by immunohistochemistry, which

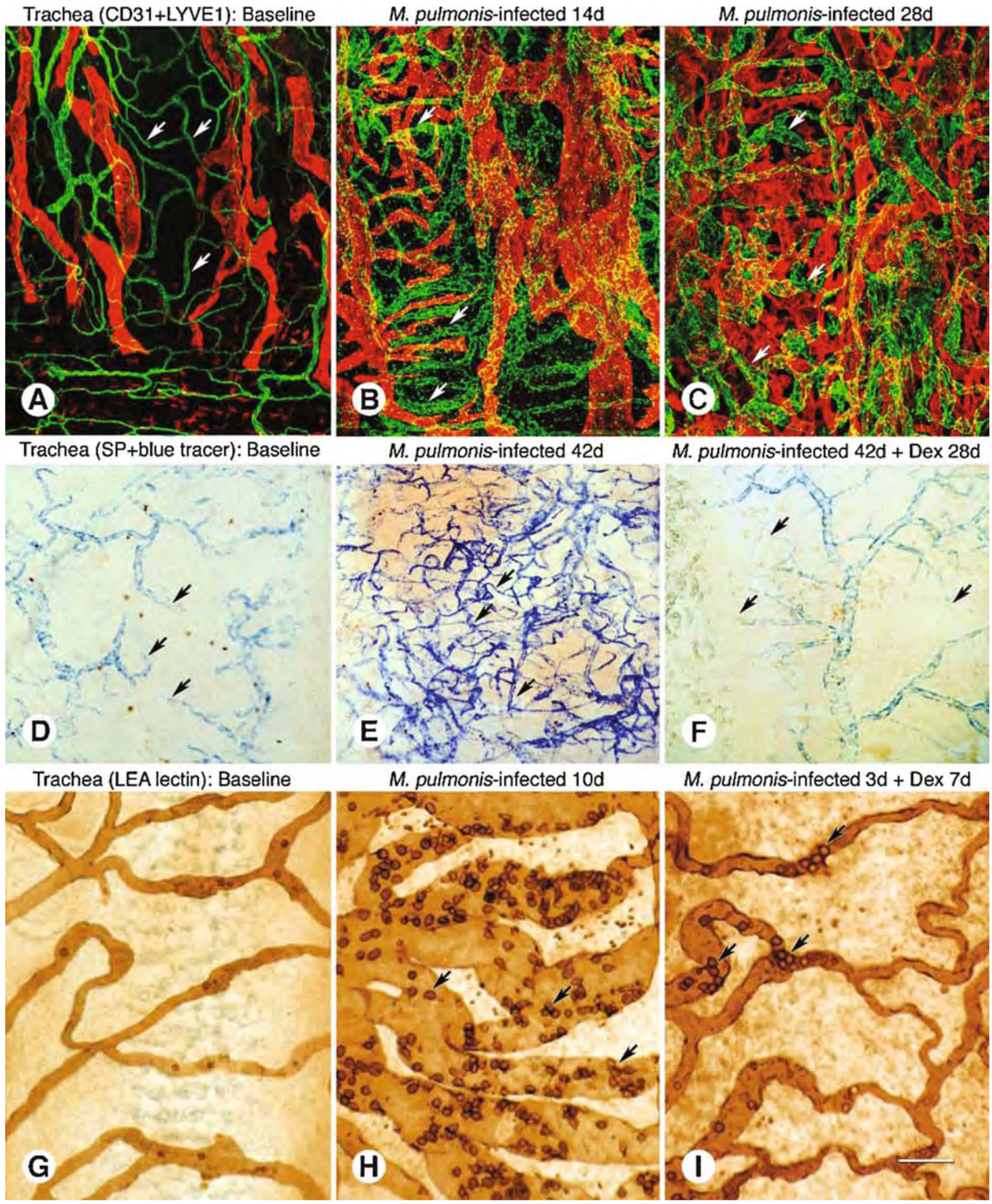

FIG. 2.3A–C. Confocal micrographs of tracheal blood vessels stained for CD31 (*green*) and lymphatics stained for LYVE-1 (*red*) showing angiogenesis and lymphangiogenesis after *M. pulmonis* infection in C3H mice: pathogen-free (**A**), infected for 14 days (**B**), or infected for 28 days (**C**) (from [23]). **D–F** Light micrographs comparing number of leaky tracheal blood vessels, marked by extravasated Monastral blue after substance P (5 µg/kg iv), in three groups of rats: pathogen-free (**D**), infected with *M. pulmonis* for 6 weeks and then saline-treated for 4 weeks (**E**), or infected with *M. pulmonis* for 6 weeks and then treated with dexamethasone (0.5 mg/kg/day ip) for 4 weeks (**F**) (from [17]). In pathogen-free rat, blue labeling begins abruptly (*arrows*) at the junction of capillaries and postcapillary venules (**D**). After infection, the number of blue vessels is strikingly increased (**E**), but blue vessels return to baseline after treatment with dexamethasone (**F**) (from [17]). **G–I.** Tracheal vasculature perfused with biotinylated LEA lectin to show vascular enlargement after *M. pulmonis* infection and reversal by dexamethasone in C3H mice: pathogen-free (**G**), infected with *M. pulmonis* for 10 days (**H**), or infected for 10 days and treated with dexamethasone (0.2 mg/day, ip) for final 7 days (**I**) (from [19]). *Arrows* mark adherent intravascular leukocytes (**H, I**). *Scale bar*: 100 µm in (**A–F**); 50 µm in (**G–I**).

make it easy to identify changes at the cellular level and to localize specific molecules [31, 38].

As another approach, fluorescent lectins that selectively bind to the luminal surface of blood vessels after iv injection can unambiguously mark the vasculature of tumors (Fig. 2.4A) [7, 40]. Fluorescent 50–100 nm cationic liposomes also label endothelial cells of tumor vessels [41]. Functional blood vessels can be distinguished from lumenless endothelial sprouts and extravascular blood lakes by using a sequence of lectin labeling, vascular perfusion of fixative, and ex vivo immunohistochemistry (Fig. 2.4A, B). The lectin labels functional vessels, vascular perfusion washes blood from the circulation, fixing extravasated erythrocytes in place, and CD31 staining marks all endothelial cells regardless of whether they are organized into blood vessels and have a lumen [40].

The distribution of endothelial cells in tumors, determined by CD31 immunoreactivity, is more complex than the vessel pattern shown by lectin binding (Fig. 2.4A, B). Although the overall arrangement of vessels is similar, more structures have CD31 immunoreactivity than are stained by lectin (Fig. 2.4A, B). Thin sprouts, not detectable by lectin staining (Fig. 2.4A), radiate from the wall of some vessels (Fig. 2.4B). Similar sprouts are evident by scanning electron microscopy (EM) in perivascular sleeves of viable tumor (Fig. 2.4C).

Vascular architecture, caliber, and density differ markedly in different types of tumors, but a consistent feature is defective or absent arteriole–capillary–venule hierarchy typical of normal organs. RIP-Tag2 tumors have unusually abundant, densely packed, anastomotic, capillary-size blood vessels (mean diameter, 8 μm) [42]. In MCa-IV tumors, capillary-size vessels are mixed with extremely large vessels; vessel diameters range from 8 μm to 294 μm (mean diameter, 45 μm) [42]. Lewis lung carcinomas have blood vessels intermediate in size between the other tumors (mean diameter, 31 μm) [42].

Endothelial Cells of Tumor Vessels

Blood vessels of tumors are lined by endothelial cells that have diverse abnormalities in gene expression, structure, and function [2, 32, 40]. The endothelial cells vary in size and thickness, and some have an irregular shape, ruffled margins, or cytoplasmic processes (Fig. 2.4D). Long projections of some endothelial cells overlap other endothelial cells, span the luminal surface of neighboring cells, or bridge the lumen (Fig. 2.4D).

Defects in the endothelial monolayer make tumor vessels leaky. Some endothelial cells are partially detached, do not form a uniformly intact barrier, or form multiple incomplete layers. Extravasated erythrocytes are a prominent manifestation of the defect in endothelial barrier function. In RIP-Tag2 tumors, erythrocyte extravasation is extensive, and blood lakes form [40]. Blood lakes resemble large, sack-like blood vessels or sinusoids, but are not continuously connected to the circulation, as shown by lack of labeling after LEA lectin and cationic liposomes were injected as tracers [40]. Round or oval openings, as large as an erythrocyte (Fig. 2.4E), and narrow slit-like spaces, are present between endothelial cells of many tumor vessels [40]. Transcellular holes 200–900 nm in diameter (Fig. 2.4E) and diaphragm-covered fenestrae 50–80 nm in diameter are also present.

Endothelial sprouts, rarely seen in quiescent blood vessels, are abundant in tumor vessels, where sprouts as long as 70 μm project from the endothelium. Sprouts are broadest at their base, taper toward a blind ending, and have filopodia at the tip (Fig. 4F-H). LEA lectin injected into the bloodstream stains only the proximal portion of sprouts (Fig. 2.4A). Filopodia are stained by GSL-I isolectin B4 [43].

Pericytes of Tumor Vessels

All normal blood vessels have mural cells that are tightly associated with endothelial cells within a common sleeve of basement membrane. Pericytes are the mural cells of capillaries and venules; smooth muscle cells are the mural cells of other blood vessels. Smooth muscle cells are readily identified by the presence of α-SMA and other muscle-related proteins, but pericytes are heterogeneous and do not consistently express a single protein that can be used for identification. Most pericytes have immunoreactivity for one or more of four markers: α-smooth muscle actin (α-SMA), platelet derived growth factor receptor-β (PDGFR-β), desmin, or chondroitin sulfate proteoglycan NG2 (NG2, CSPG4, HMW-MAA) [42, 44]. Pericytes on normal capillaries typically cover only a small proportion of the endothelial surface, have multiple long, branched cytoplasmic processes, are oriented along the vessel's longitudinal axis, and have desmin and/or NG2 but not α-SMA immunoreactivity (Fig. 2.5A).

Pericytes on tumor vessels have an abnormally loose association with endothelial cells (Fig. 2.5B) [42]. The difference in pericyte-endothelial cell association is particularly conspicuous in scanning EM views of the cell surface (Fig. 2.5C, D). Pericytes in tumors have an irregular shape (Fig. 2.5D) and may have cytoplasmic processes that accompany endothelial sprouts or project away from the vessel wall into the tumor parenchyma [42].

Pericytes in many tumors have abnormal expression of α-SMA. Pericytes on capillaries of normal pancreatic islets do not express α-SMA but do express desmin. However, pericytes in RIP-Tag2 tumors, which develop from islets, express α-SMA as well as desmin [42]. Some tumors contain cells that are morphologically similar to pericytes and are immunoreactive for α-SMA, desmin, or PDGFR-β but have no apparent association with blood vessels. Pericytes that lack a vessel association but are accompanied by basement membrane may be remnants of degenerated tumor vessels.

Basement Membrane of Tumor Vessels

Vascular basement membrane, marked by immunohistochemical staining for type IV collagen, laminin, fibronectin, or nidogen (entactin), is present on all normal blood vessels

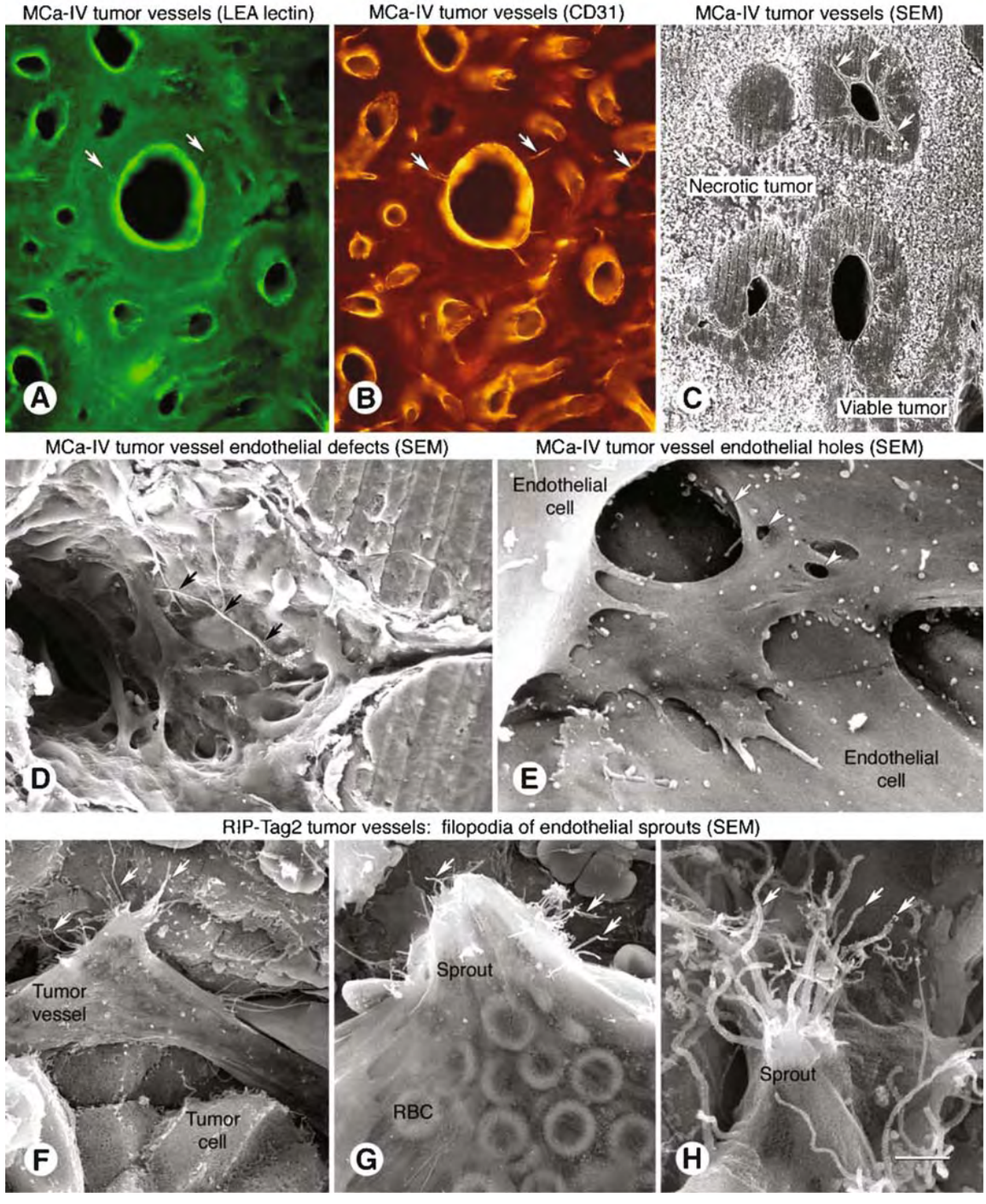

FIG. 2.4A–C. Blood vessels in MCa-IV tumors visualized by green fluorescent LEA lectin (**A**), CD31 immunoreactivity (**B**), or scanning EM (**C**) (from [40]). Both lectin and CD31 immunoreactivity mark most of the tumor vessels, but, unlike LEA lectin, CD31 also marks lumenless endothelial sprouts (*arrows*) radiating away from the vessel wall. Scanning EM shows similar sprouts (*arrows*) radiating into perivascular sleeve of tumor tissue. Necrotic tumor surrounds the perivascular sleeves of viable tumor. Scanning EM of luminal surface of blood vessel in MCa-IV tumor showing multiple abnormalities (**D**), including disorganized endothelial cells with bridges, tunnels, and 50-µm long cellular projection (*arrows*) (from [40]). Pathways for extravasation (**E**) through intercellular openings (*arrow*) and transcellular holes (*arrowheads*) in endothelium of MCa-IV tumor vessel (from [40]). Scanning EM views of sprouts with filopodia (**F–H** *arrows*) projecting from the abluminal surface of endothelial cells of blood vessels in RIP-Tag2 tumors (from [32]). *Scale bar* 150 µm in (**A,B**); 100 µm in (**C**); 15 µm in (**D**); 2.5 µm in (**E**); 10 µm in (**F**); 5 µm in (**G**); 2 µm in (**H**).

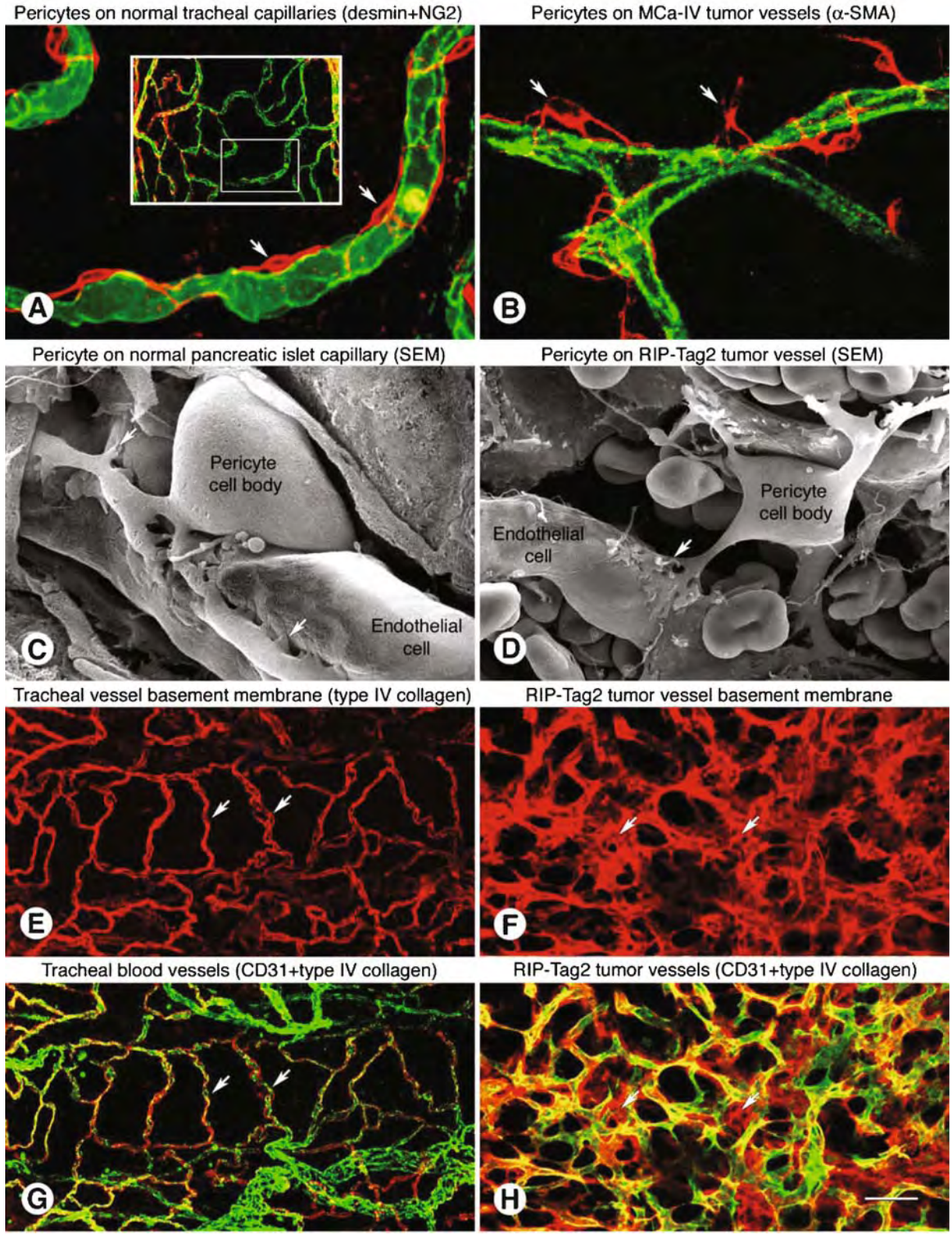

FIG. 2.5A,B. Confocal microscopic images contrasting pericytes (*red*, desmin/NG2) that are tightly associated with normal capillary in mouse trachea (**A**) (from [20]), and pericytes (*red*, α-SMA) that are loosely associated with tumor vessels in Lewis lung carcinoma (**B**) (from [49]). Endothelial cells (*green*, CD31). **A** (*inset*). Overview of tracheal vasculature showing region (*box*) enlarged in (**A**). **C,D** Scanning EM images of a pericyte closely associated with the endothelium of a normal capillary in mouse pancreatic islet (**C**) and a pericyte loosely associated with a blood vessel in RIP-Tag2 tumor (**D**). **E–H.** Confocal micrographs comparing basement membrane (*red*) of capillaries of normal adult mouse trachea (**E,G** *arrows*) (from [49]) and tortuous, anastomotic vasculature of RIP-Tag2 tumor (**F,H** *arrows*) after staining for type IV collagen immunoreactivity alone (**E,F** *red*) or with CD31 immunoreactivity (**G,H** *green*). Some type IV collagen in the tumor does not colocalize with CD31 (*arrows*). *Scale bar*: 20 μm in (**A,B**); 5 μm in (**C,D**); 50 μm in (**E–H**).

(Fig. 2.5E) and on most blood vessels in tumors (Fig. 2.5F) [45]. Type IV collagen immunoreactivity tends to be the most selective for marking vascular basement membrane in tumors [45]. Because of the close association of basement membrane with the abluminal surface of endothelial cells, sleeves of type IV collagen faithfully match the pattern of CD31 in normal organs and thereby reflect the vascular architecture (Fig. 2.5G). A uniform sleeve of type IV collagen tightly envelopes endothelial cells and pericytes, forming a sandwich with little or no space between the layers.

The basement membrane of tumor vessels has multiple abnormalities. The layer of type IV collagen is variable in thickness and has broad extensions and other irregularities not found in normal vessels. Still, tumor vessels are almost completely covered by basement membrane [45]. Interruptions in type IV collagen represent less than 2% of the endothelial surface. The largely complete basement membrane visible by immunofluorescence contrasts with reports of incomplete basement membrane on tumor vessels from EM studies. The difference may be based on methods of preservation, staining, or sampling.

Some tumor vessels have spikes or extra layers of basement membrane not in close contact with endothelial cells, which give a fuzzy outline to tumor vasculature after type IV collagen staining (Fig. 2.5F, H) [45, 46]. Spaces between layers of type IV collagen, CD31, and α-SMA reflect the loose association of endothelial cells and pericytes (Fig. 2.5B, D). Projections of basement membrane away from tumor vessels may accompany endothelial sprouts or pericyte processes [45, 46]. Multiple layers of basement membrane on tumor vessels probably result from repeated cycles of disorganized vascular growth and regression.

Cellular Actions of VEGF Inhibitors on Tumor Blood Vessels

With the goal of obtaining a better understanding of the cellular actions of angiogenesis inhibitors on tumor vessels, we took advantage of the imaging methods described earlier in the chapter and the known abnormalities of endothelial cells, pericytes, and vascular basement membrane [40, 42, 45]. Agents that block VEGF signaling were used to exploit the availability of well characterized inhibitors and detailed knowledge of VEGF ligands, VEGF receptors, and downstream signaling pathways [47, 48]. Two agents that inhibit VEGF signaling through different mechanisms had comparable effects: AG-013736 is a small molecule inhibitor of VEGF receptors and related tyrosine kinase receptors; VEGF-Trap is a decoy construct of the extracellular domain of VEGFR1 and VEGFR-2 that inhibits VEGF signaling by selectively binding the ligands [49]. Changes in tumor vessels during the first week of treatment were sought to distinguish direct effects of the agents from secondary changes.

Tumor Vascularity

Treatment with AG-013736 or VEGF-Trap causes rapid and robust changes in endothelial cells of blood vessels of RIP-Tag2 tumors (Fig. 2.6A) and in Lewis lung carcinomas. Vascular sprouting is suppressed, endothelial fenestrations disappear, patency is lost and blood flow ceases in some vessels, and tumor vascularity decreases. A slight decrease in vascularity is evident at 1 day (Fig. 6B). The reduction is larger at 2 days (Fig. 2.6C), much greater at 7 days (Fig. 2.6D), and tends to plateau thereafter. The amount of vascular regression at 7 days is greater in RIP-Tag2 tumors (70% reduction of tumor vessels) than in Lewis lung carcinomas (50% reduction). Prolongation of treatment to 21 days does not further reduce vascularity but can reduce tumor volume of RIP-Tag2 tumors [49].

Vessel Patency

How can endothelial cells of tumor vessels die without causing hemorrhage? One explanation is that vessels close and lose patency before endothelial cells regress. Under baseline conditions, most blood vessels in RIP-Tag2 tumors are patent and functional as shown by LEA lectin labeling (Fig. 2.6E) [49]. After 1 day of treatment with AG-013736 or VEGF-Trap, about 30% of tumor vessels lack lectin staining despite the continued presence of endothelial cells (Fig. 2.6F) [49]. The number of non-functional tumor vessels is maximal at 2 days and falls nearly to zero by 7 days [49]. At 7 days, only about 30% of tumor vessels remain, and the amounts of lectin staining and CD31 immunoreactivity again match. These findings fit a model whereby tumor vessels lose patency before they degenerate, and most vessels still present after a week are functional.

Endothelial Sprouts

Endothelial sprouts tipped by filopodia are abundant on blood vessels in untreated tumors (Fig. 4F-H), but are rare on tumor vessels after treatment with AG-013736. Tumor vessels that survive the treatment are less tortuous, more uniform in caliber, and have fewer sprouts and branches.

Endothelial Fenestrations

Blood vessels of many tumors including those in RIP-Tag2 mice have abundant endothelial fenestrations [40, 49, 50]. These diaphragm-covered pores are also common in normal endocrine glands, intestinal mucosa, choriocapillaris, and certain other organs [51]. The number of fenestrations in tumor vessels rapidly decreases after inhibition of VEGF signaling. Treatment with AG-013736 or VEGF-Trap reduces the number of endothelial fenestrations by about 90% at 1 day and 98% at 7 days [49]. The greater effect of inhibitors of VEGF signaling on heavily fenestrated blood vessels in RIP-Tag2 tumors, compared to non-fenestrated blood vessels in Lewis lung carcinoma, raises the possibility that

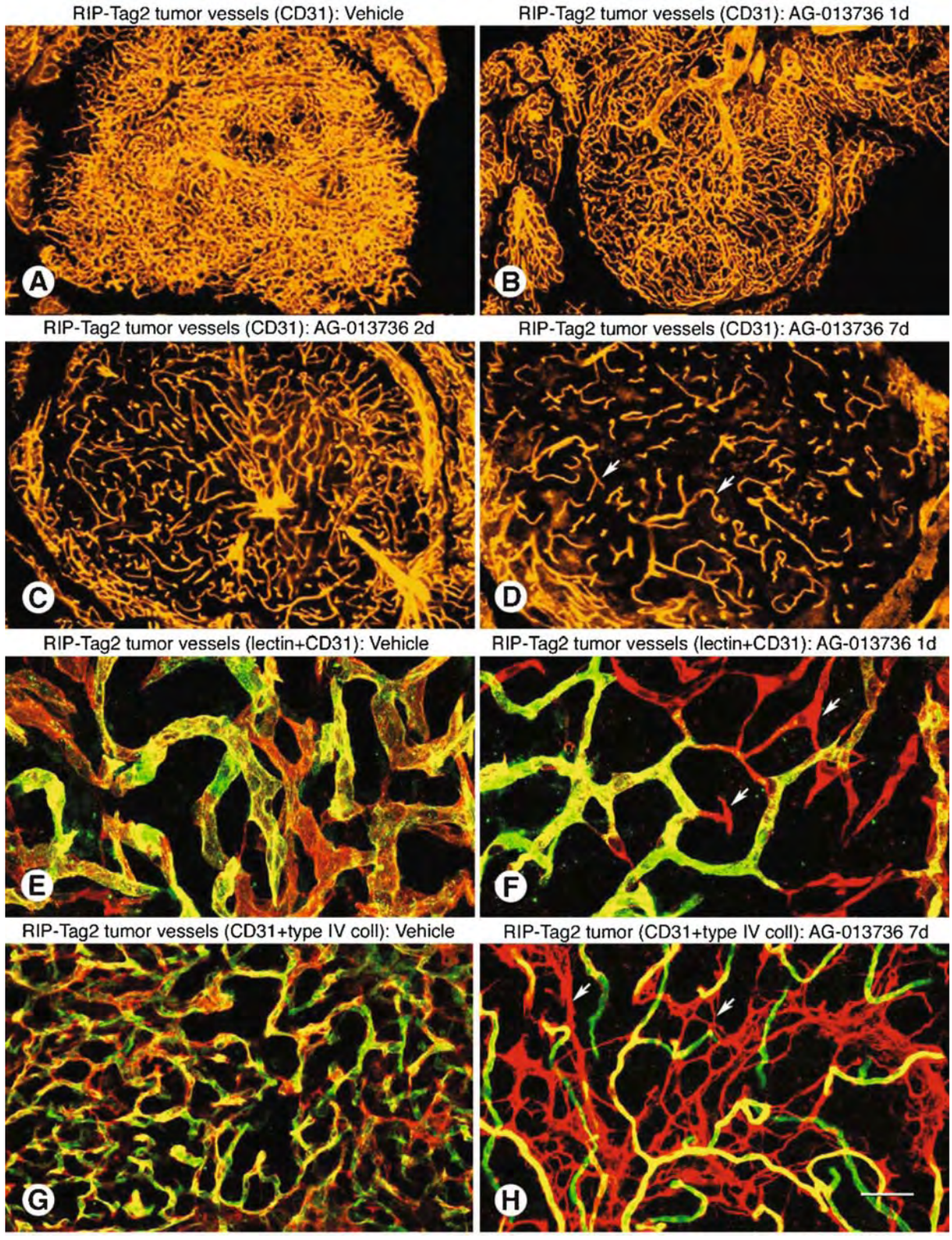

FIG. 2.6A–D. Time course of decrease in vascularity of RIP-Tag2 tumors after inhibition of VEGF signaling by AG-013736. Fluorescence microscopic images of CD31 immunoreactivity showing dense tumor vasculature under baseline conditions (**A,** vehicle treatment) and decreasing vascularity after AG-013736 for 1 day (**B**), 2 days (**C**), or 7 days (**D**) (from [49]). **E,F** Confocal microscopic images of blood vessels in RIP-Tag2 tumors after vehicle (**E**) or AG-013736 (**F**) for 1 day. LEA lectin injected iv before fixation (from [49]). Lectin staining (*green*) of blood vessels in vehicle-treated tumor largely coincides with CD31 immunoreactivity (*red*). However, after treatment with AG-013736, some vessels (*arrows*) have CD31 immunoreactivity but lack lectin staining, and thus are *red* (**F**), indicating loss of vessel patency (from [49]). **G,H** Persistence of vascular basement membrane after endothelial cells degenerate. Confocal micrographs show colocalization of CD31 (*green*) and type IV collagen (*red*) in vasculature of RIP-Tag2 tumor at baseline (**G**). After AG-013736 for 7 days, sleeves of type IV collagen devoid of CD31 (*arrows*) are abundant between surviving, normalized blood vessels (*yellow*) in RIP-Tag2 tumor (**H** *arrows*). *Scale bar*: 200 μm in (**A–D**); 25 μm in (**E,F**); 50 μm in (**G,H**).

presence of endothelial fenestrations is predictive of response to inhibition of VEGF.

VEGFR Immunoreactivity

Another consistent effect of inhibitors of VEGF signaling is reduction in expression of VEGFR-2 and VEGFR-3, reflected by reduced immunofluorescence [20, 46, 49, 51]. This change does not reflect generalized effects on membrane proteins because immunoreactivities for CD31, CD105, and PDGFR-β do not change significantly [49]. The decrease in VEGFR-2 fluorescence appears to reflect a change in epitope density on individual vessels rather than reduced vessel caliber [49]. The reduction of VEGFR-2 in endothelial cells of Lewis lung carcinoma is smaller than RIP-Tag2 tumors. To the extent that brightness of fluorescence reflects amount of expression, vessels with the highest initial VEGFR-2 expression are most likely to be destroyed or normalized into vessels with lower VEGFR-2 expression [49].

Pericytes

Inhibition of VEGF signaling results in a much larger reduction in tumor vessels than in pericytes [49]. After treatment of RIP-Tag2 tumors and Lewis lung carcinomas with AG-013736 or VEGF-Trap, twice as many pericytes remain as tumor vessels. Surviving pericytes have two fates in the short-term. Some become more tightly associated with endothelial cells, even oriented circumferentially around vessels in a fashion resembling smooth muscle cells on arterioles [49]. Others, identified as cells expressing pericyte markers surrounded by basement membrane, have no apparent association with tumor vessels [49]. The long-term fate of the latter cells is unknown.

Basement Membrane

Blood vessels of RIP-Tag2 tumors, like those in most other tumors, are covered by basement membrane (Fig. 6G) [45, 49]. After treatment with AG-013736 or VEGF-Trap for 7 days, distinctive strands of type IV collagen unaccompanied by endothelial cells are scattered throughout the tumor (Fig. 6H). When tumor vascularity decreases more than 75%, basement membrane decreases at most 30%. Empty strands of basement membrane become more abundant as tumor vessels regress during treatment and remain for at least three weeks [49]. Empty sleeves of basement membrane are not stained by lectin or endothelial cell markers and are not perfused with blood [49].

Rapid Regrowth of Tumor Vessels After Cessation of VEGF Inhibitor

Tumor vessels regrow rapidly after cessation of VEGF inhibition. In RIP-Tag2 tumors, overall vascularity decreases 60–75% during treatment with AG-013736 for 7 days (Fig. 2.7A, B) [46, 49]. After the inhibitor is stopped, tumor vascularity nearly doubles during the first 4 days and returns to the baseline condition in 7 days (Fig. 2.7C, D) [46]. Tumor vascularity does not exceed the baseline even after longer periods of regrowth. Vascular regrowth is at least as rapid in Lewis lung carcinomas, where the 50% reduction in vascularity is completely reversed within 4 days [46].

Regrowing tumor vessels become functional almost as rapidly as they regrow [46]. LEA lectin injected iv to label patent blood vessels marks nearly all vessels in untreated RIP-Tag2 tumors (Fig. 2.7E). After AG-013736 for 7 days, surviving tumor vessels are sparse but all have lectin labeling (Fig. 2.7F). One day after the treatment ends, sprouts are present (Fig. 2.7G, arrows). By 7 days, lectin stains almost all of the regrown vasculature (Fig. 2.7H). Lectin labeling and vascularity increase in parallel as tumor vascularity returns to baseline [46].

Tumor vessels sensitive to VEGF inhibitors have unusually high expression of VEGFR-2. Inhibition of VEGF signaling by AG-013736 leads to a reduction in VEGFR-2 immunofluorescence [46, 49]. After the inhibition is withdrawn, VEGFR-2 immunofluorescence returns to baseline in regrown tumor vessels during the first week.

Regrown tumor vessels reacquire VEGF dependence within a week after treatment ends [46]. Treatment with a second round of AG-013736 beginning 7 days after the first round reduces tumor vascularity as much as the first round.

Treatment with AG-013736 reduces by about one-third the population of α-SMA-positive pericytes in RIP-Tag2 tumors [46, 49]. This reduction reverses rapidly and is fully back to baseline within 4 days after the treatment ends. PDGFR-β immunoreactivity does not undergo a corresponding reduction during treatment, suggesting that AG-013736 induces a reversible change in pericyte phenotype, characterized by reduction in α-SMA expression, rather than a decrease in number of pericytes. AG-028262, a potent small molecule inhibitor of VEGFR-2 phosphorylation with little action on PDGFR-β, has similar effects on α-SMA expression [46]. These results fit with the change in pericyte phenotype being a downstream consequence of inhibition of VEGFR signaling, rather than a direct effect on PDGF signaling.

Regression of endothelial cells after inhibition of VEGF signaling leaves pericytes in otherwise empty sleeves of basement membrane [46]. In untreated tumors, endothelial cells and vascular basement membrane have similar distributions (Fig. 7I). After 7 days of AG-013736, the overall pattern of basement membrane changes little, despite the marked decrease in tumor vascularity (Fig. 2.7J). By 7 days after the treatment ends, tumor vasculature returns to baseline and empty sleeves of basement membrane disappear (Fig. 7K) [46].

The abundance of empty sleeves of basement membrane left behind by regressing tumor vessels and the apparent lack of duplication of vascular basement membrane during regrowth point to the possibility that the sleeves serve as a scaffold for regrowing tumor vessels. Consistent with this process, the rate of vessel regrowth is similar to the rate of disappearance of the

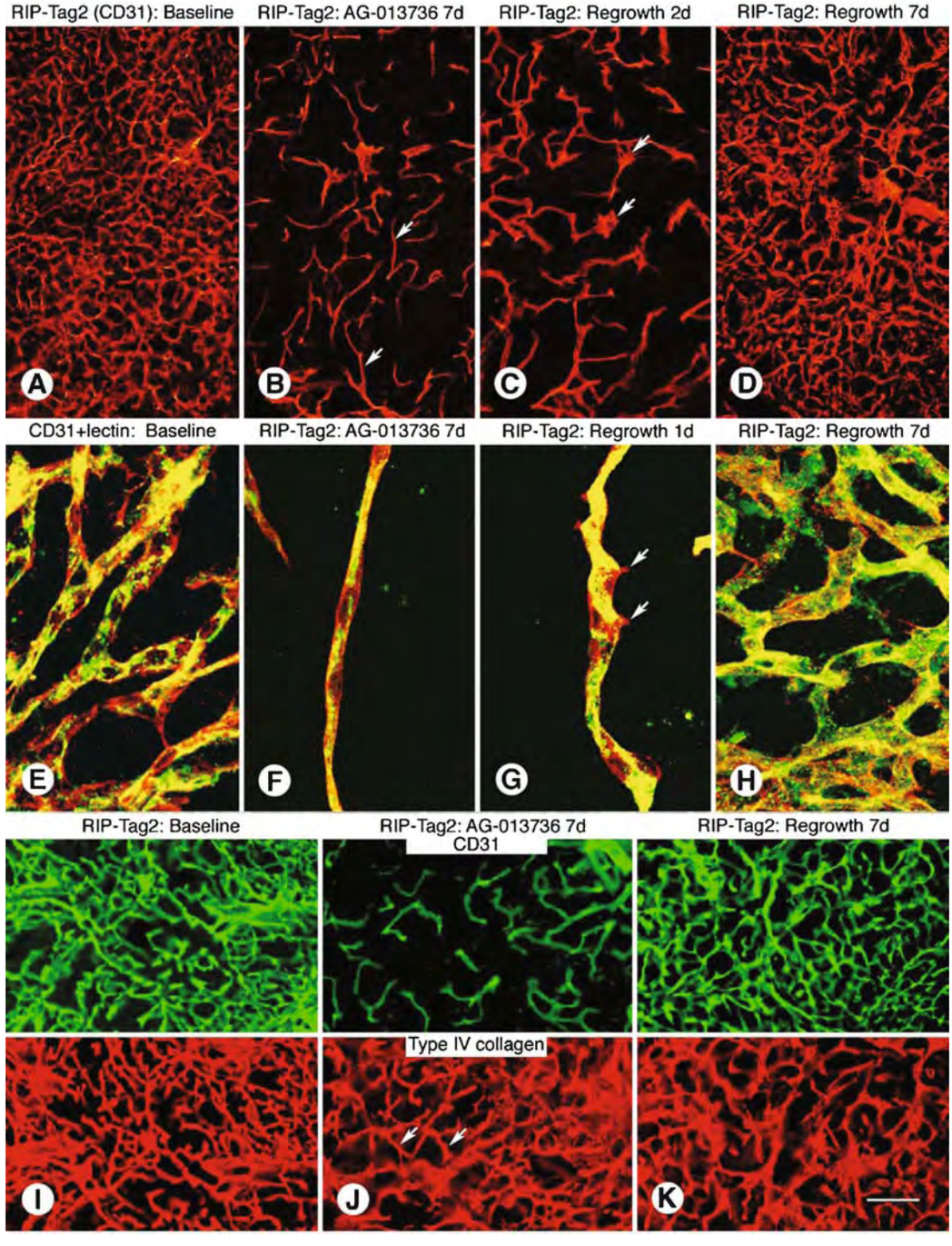

FIG. 2.7A–D. Regrowth of tumor vessels after cessation of VEGF inhibition. Confocal micrographs of RIP-Tag2 tumors stained for CD31 immunoreactivity (*red*) comparing vascularity of untreated tumor (**A**), tumor after AG-013736 for 7 days (**B**), and tumor after AG-013736 was stopped for 2 days (**C**) or 7 days (**D**) (from [46]). By 7 days, tumor vessels are as abundant as at baseline. **E–H** Confocal micrographs of RIP-Tag2 tumors comparing vessels, labeled by iv green fluorescent LEA lectin and then stained for CD31 immunoreactivity, at baseline (**E**), AG-013736 for 7 days (**F**), or after AG-013736 was stopped for 1 day (**G**) or 7 days (**H**) (from [46]). In the untreated tumor (**E**), almost all blood vessels are labeled with lectin. After AG-013736 for 7 days (**F**), surviving tumor vessels have lectin labeling. At 1 day after treatment ended nearly all vessels are stained with lectin, but lectin-negative sprouts (*red*) are present (**G** *arrows*). At 7 days after treatment ended (**H**), lectin and CD31 staining resembles the baseline (**E**). **I–K.** Fluorescence microscopic images of tumors showing CD31-positive endothelial cells (*green*, *upper*) and type IV collagen-positive basement membrane (*red*, *lower*) at baseline (**I**), after AG-013736 for 7 days (**J**), and 7 days after end of 7-day treatment (**K**) (from [46]). The two markers have similar distributions in untreated RIP-Tag2 tumors (**I**), but after AG-013736, CD31-positive vessels are sharply reduced but basement membrane is not (**J**). By 7 days after treatment ended, tumor vascularity is restored, and patterns of CD31 and type IV collagen again match (**K**). *Scale bar*: 150 µm in (**A–D**); 25 µm in (**E–H**); 120 µm in (**I–K**).

empty sleeves [46]. Sleeves of basement membrane, which are sites of bound VEGF, may facilitate the rapid revascularization of tumors [46].

Effects of VEGF Inhibitors on Normal Blood Vessels

The essential role of VEGF during embryonic development has been assumed not to persist into adult life. Yet VEGF has actions in normal organs of the adult, including effects on the structure, function, and survival of some blood vessels, on blood pressure regulation, and on renal, neurological, and hepatic function [51, 52]. Functions of VEGF in normal organs provide insight into mechanisms of side effects in cancer patients treated with VEGF inhibitors [52].

Inhibition of VEGF signaling is accompanied by multiple changes in normal capillaries of certain organs. These include reduction in endothelial fenestrations, reduction in endothelial cell expression of VEGFR-2 and VEGFR-3, and regression of capillaries [51]. Endothelial fenestrations are a feature of capillaries in gastrointestinal tract, many endocrine organs, kidney, liver, choroid plexus, and choriocapillaris [51]. Fenestrations begin to go away within 24 h of inhibition of VEGF signaling [49]. After 2 or 3 weeks, the number of fenestrations is conspicuously reduced in capillaries of pancreatic islets (Fig. 2.8A, B), renal glomerulus (Fig. 2.8C, D), and thyroid, where fenestrations decrease by as much as 88% [51].

Inhibition of VEGF signaling leads to regression of capillaries in the trachea (Fig. 2.8E), villi of small intestine (Fig. 2.8F, G), pancreatic islets, thyroid (Fig. 2.8H, I), adrenal cortex, pituitary, choroid plexus, and adipose tissue [51, 53]. The amount of regression is dose-dependent and varies from organ to organ, with a maximum of 68% in thyroid [51]. In these experiments, little or no capillary regression was found in brain, retina, skeletal muscle, cardiac muscle, or lung [49, 51].

After inhibition of VEGF signaling for only 1 day, fibrin accumulates and patency is lost in some capillaries [20, 49, 53]. By 2 days, endothelial cells undergo apoptosis and regression. The magnitude of capillary loss decreases with age, ranging from 39% at 4 weeks of age, 28% at 8 weeks, to 14% at 16 weeks [20]. Empty sleeves of basement membrane persist for weeks after endothelial cells regress (Fig. 2.8E) [46].

Most capillaries in the thyroid grow back within 1 or 2 weeks (Fig. 2.8H-J) [46]. Tracheal capillaries also regrow rapidly [53]. As in tumors, regrowth appears to be facilitated by if not dependent on empty sleeves of basement membrane that provide a scaffold for revascularization [46].

Together, these findings show the dependency on VEGF signaling of endothelial fenestrations and survival of normal fenestrated capillaries [49, 51]. They also show the potential plasticity of the microvasculature [51]. Importantly, these observations raise the possibility that blood vessels having abundant endothelial fenestrations and high VEGFR-2 expression are especially sensitive to inhibitors of VEGF signaling. Reduction in endothelial fenestrations and VEGFR-2 are responses to VEGF inhibition that may serve as surrogates for predicting therapeutic efficacy [52].

Conclusions

The expanding diversity of preclinical models makes it possible to examine angiogenesis and vascular remodeling under many defined experimental conditions. Imaging techniques are being improved to complement the experimental models and make it easier to elucidate changes in endothelial cells and pericytes, obtain detailed cellular information on blood vessels of the microcirculation, and characterize alterations in the architecture of three-dimensional vascular networks. These approaches are rapidly advancing the understanding of the normal microvasculature and the diverse changes blood vessels undergo in disease.

With the recognition that angiogenesis and vascular remodeling occur under many conditions, it seems reasonable to assume that they are generic processes with similar properties regardless of disease pathophysiology. While this probably is true at some level, blood vessels change in strikingly different ways in different diseases. New and remodeled blood vessels at sites of inflammation acquire features specialized to support increased blood flow and regulated influx of inflammatory cells. Capillaries in inflamed tissues develop a phenotype resembling that of venules, with up-regulation of endothelial cell receptors for inflammatory mediators that initiate vessel leakiness and leukocyte influx. Leakage from these vessels occurs though focal gaps that form reversibly between endothelial cells. Adhesion molecules expressed on the remodeled endothelial cells participate in the orchestrated process of leukocyte rolling, attachment, and migration.

Unlike the changes in inflammation, endothelial cells of tumor vessels undergo disorganized sprouting and proliferation, overexpress or underexpress membrane receptors, and may become dependent on VEGF or other growth factors for survival. Structural defects result in impaired endothelial barrier function, poor blood flow, high interstitial pressure, and altered immune cell entry. Functional abnormalities of tumor vessels can restrict blood flow to growing tumor cells despite rich vascularity. Poor blood flow can promote invasion and result in hypoxia and cell death. Robust angiogenesis and expansion of tumor cells can paradoxically occur adjacent to regions of necrosis.

Abnormalities of blood vessels can be exploited in diagnosis and treatment of inflammation and tumors. Reversal of environmental factors that induce the abnormal vascular phenotype can lead to clinical improvement. When factors that promote VEGF signaling contribute to blood vessel abnormalities in tumors, inhibition of VEGF signaling can stop angiogenesis and promote vascular regression or normalization. Empty sleeves of basement membrane left behind after tumor vessels regress provide a scaffold for revascularization. As understanding of the vascular biology of inflammation and tumors advances, so will strategies for effectively blocking

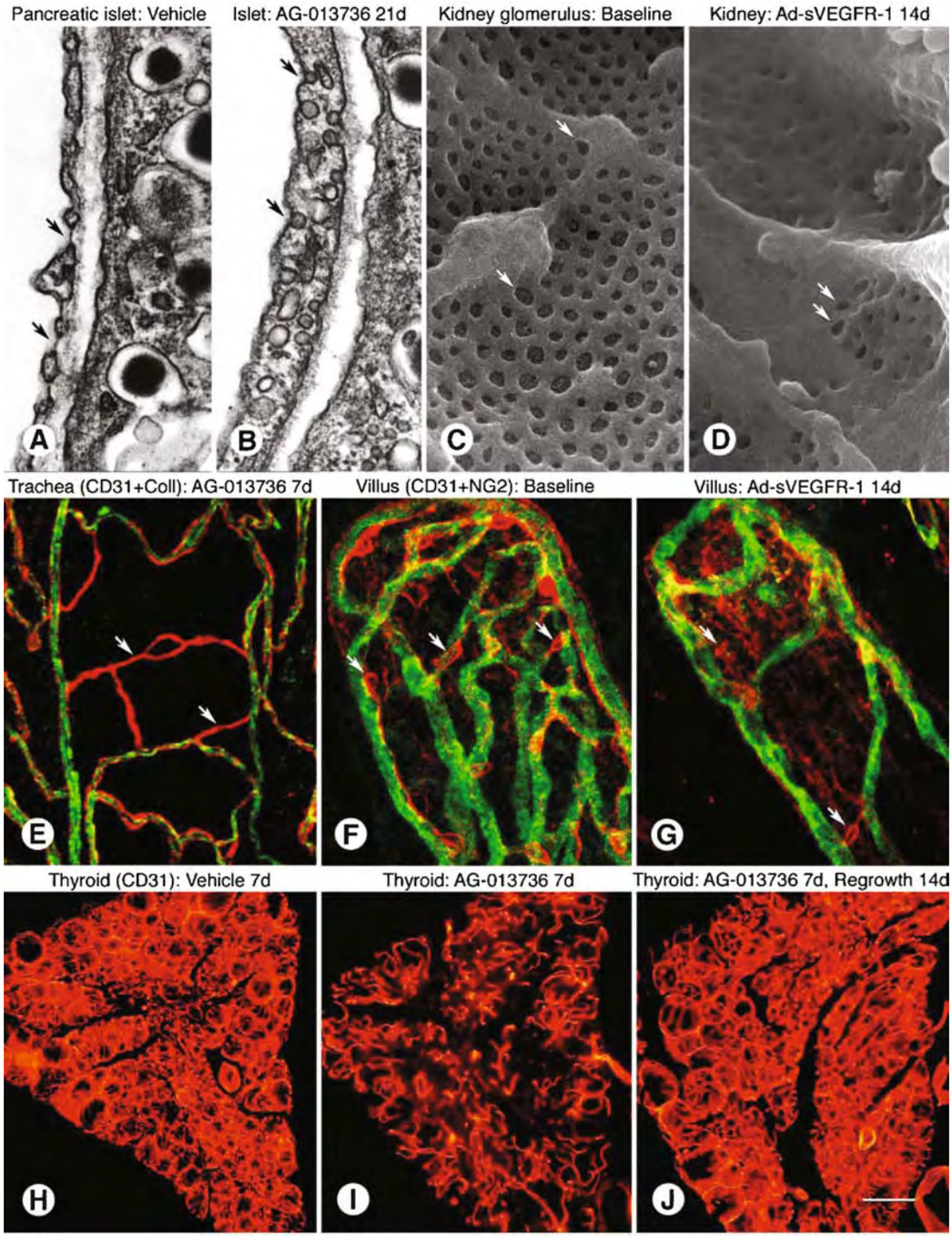

FIG. 2.8A–D. EM images showing reduction in endothelial fenestrations (arrows) after inhibition of VEGF signaling. Transmission EM images of pancreatic islet capillaries showing thin endothelium and abundant fenestrations with diaphragms under baseline conditions (**A**) compared to thick endothelium, few fenestrations, and abundant caveolae after AG-013736 for 21 days (**B**) (from [51]). **C,D** Scanning EM images of luminal surface of renal glomerular capillaries showing abundant endothelial fenestrations under baseline conditions (**C**) and few fenestrations after adenovirally delivered soluble VEGFR1 (Ad-sVEGFR-1) for 14 days (**D**) (from [51]). **E** Confocal micrograph showing capillary regression in mouse trachea after inhibition of VEGF signaling by AG-013736 for 7 days (from [49]). Type IV collagen (*red*); CD31 (*green*). Empty sleeves of basement membrane (*red*, *arrows*) are left behind where capillaries regressed (**E**). **F,G** Confocal microscopic images of capillaries in intestinal villi of normal adult mice under baseline conditions (**F**) and after inhibition of VEGF signaling by Ad-sVEGFR-1 for 14 days (**G**) (from [51]). Pericytes (*red*, NG2, *arrows*) are located on normal capillaries (**F**) and at sites where capillaries have regressed (**G**). **H–J**. Regression of thyroid capillaries after inhibition of VEGF signaling followed by rapid regrowth after end of treatment (from [51]). Fluorescence micrographs of CD31 immunoreactivity show dense vascularity of thyroid follicles under baseline conditions (**H**), loss of half of the capillaries after AG-013736 for 7 days (**I**), and complete vascular regrowth over 14 days after end of treatment (**J**). *Scale bar*: 0.3 µm in (**A,B**); 0.5 µm in (**C,D**); 50 µm in (**E**); 25 µm in (**F,G**); 160 µm in (**H–J**).

angiogenesis and destroying pathological vessels or reversing the abnormal phenotype without impacting the normal vasculature.

Acknowledgments. The author thanks Hiroya Hashizume for preparing the scanning electron micrographs, Amy Haskell for the transmission electron micrographs, and Fabienne Baffert, Peter Baluk, Jeffrey Bowden, Tetsuichiro Inai, Tomomi Kamba, Michael Mancuso, Shunichi Morikawa, Scott Norberg, and Gavin Thurston for fluorescence and confocal microscopic images. The research described in this review was supported in part by National Institutes of Health grants HL24136 and HL59157 from the National Heart, Lung, and Blood Institute and CA82923 from the National Cancer Institute, and by funding from AngelWorks Foundation.

References

1. Baluk P, Falcón BL, Hashizume H, et al. Cellular actions of angiogenesis inhibitors on blood vessels. In: Marmé D, Fusenig N, eds. Tumor Angiogenesis: Basic Mechanisms and Cancer Therapy. New York: Springer; 2007:557–76.
2. Baluk P, Hashizume H, McDonald DM. Cellular abnormalities of blood vessels as targets in cancer. Curr Opin Genet Dev 2005;15(1):102–11.
3. McDonald DM, Thurston G, Baluk P. Endothelial gaps as sites for plasma leakage in inflammation. Microcirculation 1999;6(1):7–22.
4. Thurston G, Baluk P, McDonald DM. Determinants of endothelial cell phenotype in venules. Microcirculation 2000;7(1):67–80.
5. McDonald DM. Angiogenesis and remodeling of airway vasculature in chronic inflammation. Am J Respir Crit Care Med 2001;164(10 Pt 2):S39–45.
6. McDonald DM. Endothelial gaps and permeability of venules in rat tracheas exposed to inflammatory stimuli. Am J Physiol 1994;266(1 Pt 1):L61–83.
7. Thurston G, Baluk P, Hirata A, et al. Permeability-related changes revealed at endothelial cell borders in inflamed venules by lectin binding. Am J Physiol 1996;271(6 Pt 2):H2547–62.
8. Thurston G, Murphy TJ, Baluk P, et al. Angiogenesis in mice with chronic airway inflammation: strain-dependent differences. Am J Pathol 1998;153(4):1099–112.
9. Murphy TJ, Thurston G, Ezaki T, et al. Endothelial cell heterogeneity in venules of mouse airways induced by polarized inflammatory stimulus. Am J Pathol 1999;155(1):93–103.
10. Lindsey JR, Baker HJ, Overcash RG, et al. Murine chronic respiratory disease. Significance as a research complication and experimental production with Mycoplasma pulmonis. Am J Pathol 1971;64(3):675–708.
11. Lindsey JR, Cassell H. Experimental Mycoplasma pulmonis infection in pathogen-free mice. Models for studying mycoplasmosis of the respiratory tract. Am J Pathol 1973;72(1):63–90.
12. McDonald DM, Schoeb TR, Lindsey JR. Mycoplasma pulmonis infections cause long-lasting potentiation of neurogenic inflammation in the respiratory tract of the rat. J Clin Invest 1991;87(3):787–99.
13. Baluk P, Bowden JJ, Lefevre PM, et al. Upregulation of substance P receptors in angiogenesis associated with chronic airway inflammation in rats. Am J Physiol 1997;273(3 Pt 1):L565–71.
14. Kwan ML, Gomez AD, Baluk P, et al. Airway vasculature after mycoplasma infection: chronic leakiness and selective hypersensitivity to substance P. Am J Physiol Lung Cell Mol Physiol 2001;280(2):L286–97.
15. Davidson MK, Lindsey JR, Parker RF, et al. Differences in virulence for mice among strains of Mycoplasma pulmonis. Infection and immunity 1988;56(8):2156–62.
16. Cartner SC, Simecka JW, Lindsey JR, et al. Chronic respiratory mycoplasmosis in C3H/HeN and C57BL/6N mice: lesion severity and antibody response. Infection and immunity 1995;63(10):4138–42.
17. Bowden JJ, Schoeb TR, Lindsey JR, et al. Dexamethasone and oxytetracycline reverse the potentiation of neurogenic inflammation in airways of rats with Mycoplasma pulmonis infection. Am J Respir Crit Care Med 1994;150(5 Pt 1):1391–401.
18. Ezaki T, Baluk P, Thurston G, et al. Time course of endothelial cell proliferation and microvascular remodeling in chronic inflammation. Am J Pathol 2001;158(6):2043–55.
19. Thurston G, Maas K, Labarbara A, et al. Microvascular remodelling in chronic airway inflammation in mice. Clin Exp Pharmacol Physiol 2000;27(10):836–41.
20. Baffert F, Thurston G, Rochon-Duck M, et al. Age-related changes in vascular endothelial growth factor dependency and angiopoietin-1-induced plasticity of adult blood vessels. Circ Res 2004;94(7):984–92.
21. Baluk P, Lee CG, Link H, et al. Regulated angiogenesis and vascular regression in mice overexpressing vascular endothelial growth factor in airways. Am J Pathol 2004;165(4):1071–85.
22. Baluk P, Raymond WW, Ator E, et al. Matrix metalloproteinase-2 and -9 expression increases in Mycoplasma-infected airways but is not required for microvascular remodeling. Am J Physiol Lung Cell Mol Physiol 2004;287(2):L307–17.
23. Baluk P, Tammela T, Ator E, et al. Pathogenesis of persistent lymphatic vessel hyperplasia in chronic airway inflammation. J Clin Invest 2005;115(2):247–57.
24. Thurston G, Wang Q, Baffert F, et al. Angiopoietin 1 causes vessel enlargement, without angiogenic sprouting, during a critical developmental period. Development 2005;132(14):3317–26.
25. Cho CH, Kim KE, Byun J, et al. Long-term and sustained COMP-Ang1 induces long-lasting vascular enlargement and enhanced blood flow. Circ Res 2005;97(1):86–94.
26. Baffert F, Le T, Thurston G, et al. Angiopoietin-1 decreases plasma leakage by reducing number and size of endothelial gaps in venules. Am J Physiol Heart Circ Physiol 2006;290(1):H107–18.
27. Calvert JT, Riney TJ, Kontos CD, et al. Allelic and locus heterogeneity in inherited venous malformations. Hum Mol Genet 1999;8(7):1279–89.
28. Vikkula M, Boon LM, Carraway KL, 3rd, et al. Vascular dysmorphogenesis caused by an activating mutation in the receptor tyrosine kinase TIE2. Cell 1996;87(7):1181–90.
29. Nishimoto M, Akashi A, Kuwano K, et al. Gene expression of tumor necrosis factor alpha and interferon gamma in the lungs of Mycoplasma pulmonis-infected mice. Microbiol Immunol 1994;38(5):345–52.
30. Faulkner CB, Simecka JW, Davidson MK, et al. Gene expression and production of tumor necrosis factor alpha, interleukin 1, interleukin 6, and gamma interferon in C3H/HeN and C57BL/6N mice in acute Mycoplasma pulmonis disease. InfectImmun 1995;63(10):4084–90.
31. McDonald DM, Choyke PL. Imaging of angiogenesis: from microscope to clinic. Nat Med 2003;9(6):713–25.

32. Ocak I, Baluk P, Barrett T, et al. The biologic basis of in vivo angiogenesis imaging. Front Biosci 2007;12:3601–16.
33. Maniotis AJ, Folberg R, Hess A, et al. Vascular channel formation by human melanoma cells in vivo and in vitro: vasculogenic mimicry. Am J Pathol 1999;155(3):739–52.
34. Chang YS, di Tomaso E, McDonald DM, et al. Mosaic blood vessels in tumors: frequency of cancer cells in contact with flowing blood. Proc Natl Acad Sci U S A 2000;97(26):14608–13.
35. McDonald DM, Munn L, Jain RK. Vasculogenic mimicry: how convincing, how novel, and how significant? Am J Pathol 2000;156(2):383–8.
36. Folberg R, Maniotis AJ. Vasculogenic mimicry. Apmis 2004;112(7–8):508–25.
37. Hendrix MJ, Seftor EA, Hess AR, et al. Vasculogenic mimicry and tumour-cell plasticity: lessons from melanoma. Nature Rev 2003;3(6):411–21.
38. di Tomaso E, Capen D, Haskell A, et al. Mosaic tumor vessels: cellular basis and ultrastructure of focal regions lacking endothelial cell markers. Cancer Res 2005;65(13):5740–9.
39. Jain RK, Munn LL, Fukumura D. Dissecting tumour pathophysiology using intravital microscopy. Nature Rev 2002;2(4):266–76.
40. Hashizume H, Baluk P, Morikawa S, et al. Openings between defective endothelial cells explain tumor vessel leakiness. Am J Pathol 2000;156(4):1363–80.
41. Thurston G, McLean JW, Rizen M, et al. Cationic liposomes target angiogenic endothelial cells in tumors and chronic inflammation in mice. J Clin Invest 1998;101(7):1401–13.
42. Morikawa S, Baluk P, Kaidoh T, et al. Abnormalities in pericytes on blood vessels and endothelial sprouts in tumors. Am J Pathol 2002;160(3):985–1000.
43. Gerhardt H, Golding M, Fruttiger M, et al. VEGF guides angiogenic sprouting utilizing endothelial tip cell filopodia. J Cell Biol 2003;161(6):1163–77.
44. Sennino B, Falcon BL, McCauley D, et al. Sequential loss of tumor vessel pericytes and endothelial cells after inhibition of platelet-derived growth factor-beta by selective aptamer AX102. Cancer Res 2007;67(15):7358–67.
45. Baluk P, Morikawa S, Haskell A, et al. Abnormalities of basement membrane on blood vessels and endothelial sprouts in tumors. Am J Pathol 2003;163(5):1801–15.
46. Mancuso MR, Davis R, Norberg SM, et al. Rapid vascular regrowth in tumors after reversal of VEGF inhibition. J Clin Invest 2006;116(10):2610–21.
47. Ferrara N. Vascular endothelial growth factor: basic science and clinical progress. Endocr Rev 2004;25(4):581–611.
48. Ferrara N, Mass RD, Campa C, et al. Targeting VEGF-A to treat cancer and age-related macular degeneration. Ann Rev Med 2007;58:491–504.
49. Inai T, Mancuso M, Hashizume H, et al. Inhibition of vascular endothelial growth factor (VEGF) signaling in cancer causes loss of endothelial fenestrations, regression of tumor vessels, and appearance of basement membrane ghosts. Am J Pathol 2004;165(1):35–52.
50. Pasqualini R, Arap W, McDonald DM. Probing the structural and molecular diversity of tumor vasculature. Trends Mol Med 2002;8(12):563–71.
51. Kamba T, Tam BY, Hashizume H, et al. VEGF-dependent plasticity of fenestrated capillaries in the normal adult microvasculature. Am J Physiol Heart Circ Physiol 2006;290(2):H560–76.
52. Kamba T, McDonald DM. Mechanisms of adverse effects of anti-VEGF therapy for cancer. British journal of cancer 2007;96(12):1788–95.
53. Baffert F, Le T, Sennino B, et al. Cellular changes in normal blood capillaries undergoing regression after inhibition of VEGF signaling. Am J Physiol Heart Circ Physiol 2006;290(2):H547–59.

http://www.springer.com/978-0-387-71517-9

Angiogenesis
An Integrative Approach from Science to Medicine
Figg, W.; Folkman, J. (Eds.)
2008, XIX, 601 p., Hardcover
ISBN: 978-0-387-71517-9